# Solving the non-linear motion in a micromanipulation system powered by thermocapillary flows

Franco Basualdo, Aude Bolopion, Michaël Gauthier, Pierre Lambert

# Solving the non-linear motion in a micromanipulation system powered by thermocapillary flows

Franco N. Piñan Basualdo[1], Aude Bolopion[2], Michaël Gauthier[2] and Pierre Lambert[3]

*Abstract*—**Non-contact micromanipulation tools have emerged as a promising solution for manipulating small components. However, they are mainly based on non-linear actuation principles requiring ad-hoc control strategies. This paper proposes non-linear control laws to actuate a non-contact manipulation system based on thermocapillary flows for the manipulation of micro-objects on an air-water interface. The actuation system consists of steering a laser beam to locally heat the liquid surface, thus inducing a thermocapillary flow. The resulting flow propels floating objects away from the laser spot with a significant velocity (up to ten body-length per second) but the behavior is highly non-linear. Notably, small errors in the laser positioning are amplified and give place to non-linear motion. Therefore, we developed a control method consisting of a non-linear position controller including a laser position observer. We achieve stable 2D position control in this non-linear system, with a precision of $0.3\,\mathrm{mm}$ on a $0.5\,\mathrm{mm}$ object.**

*Index Terms*—**Automation at Micro-Nano Scales – Micro/Nano Robots – Motion Control**

## I. INTRODUCTION

**R**OBOTIC manipulation of microscale objects can be difficult since adhesion between the gripper and the object often dominates over the object's weight and inertia [1]. Therefore, non-contact manipulation methods have been developed to be able to control the position and/or trajectory of micro-objects without touching them. Non-contact actuation principles can be classified into three categories: microswimmers, field-based actuation, and flow-based actuation.

First, swimmers are those microrobots that harvest energy from the environment to propel themselves in a fluid media. For example, chemical [2]–[4], acoustic [5]–[7] and magnetic [8]–[10] phenomena can be used to power microswimmers.

The main drawback of these techniques is that they require geometrically or chemically complex robots able to transform those energy sources into movement.

Second, field-based micro-manipulation tools are those that consist in modulating a potential energy field to steer micro-objects. Various principles have been proposed in the literature such as optical tweezers [11]–[13], acoustic [14]–[16] and magnetic [17]–[20] manipulation. In general, these methods consist in controlling the position of one or several potential minima that will attract the micro-objects. Field-based methods are highly dependent on the micro-objects' physical properties (*e.g.,* magnetic susceptibility for magnetic manipulation).

Third, flow-based micro-manipulation tools consist of the generation and control of flows that would convey the micro-objects. The flow can be controlled on the entire workspace [21], [22] or only around the micro-object by generating local flows [23]–[26]. The main advantage of flow-based tools is that they can manipulate any micro-object, regardless of its material properties and geometry. However, flow-based manipulation often gives place to unstable and non-linear behaviors [23], [26], which require a non-linear controller to stabilize the trajectory and/or position of the manipulated object. In this paper, we propose an original non-linear closed-loop controller for the 2D control of micro-objects for a micromanipulation system powered by thermocapillary flows.

We have previously proposed a flow-based micro-manipulation platform to manipulate objects floating at the air-water interface [27]. Concretely, we generate a local thermocapillary flow by locally heating the interface, giving place to an interfacial flow from hot to cold areas. In particular, we use a laser as a heat source because of its large power density, which gives place to strong and localized flows [28]. The objective of these previous works was to demonstrate the relevance of this actuation principle using simple controllers. Because of the non-linear behavior, the controlled particle position had an unexpected transient response, with the particle following a convoluted trajectory to the target. In this article, we propose a more advanced control method to significantly improve the position controller performance. In particular, we develop a non-linear laser position observer that compensates for laser positioning errors. This controller improves the transitory regime of the system, making the point-to-point control more reliable and predictable.

## II. ACTUATION

### A. Principle

The actuation mechanism is based on the thermocapillary effect [29], the emergence of a flow due to a temperature gradient along a fluid interface. In our case, the temperature gradient is generated by locally heating the interface with a laser beam. The laser energy is absorbed by the fluid, thus locally increasing the temperature, and locally decreasing the surface tension. This surface tension unbalance gives rise to an interfacial flow from hot to cold areas (radially away from the laser spot). A more detailed description of the generated flow can be found in [28].

In this work, we exploited the thermocapillary phenomena for the actuation of particles floating on the surface of a fluid layer. We used a laser-powered thermocapillary flow to convey floating particles away from the laser spot as, shown in Fig. 1. The particles can be controlled by steering the laser spot on the interface. To estimate the required laser spot position, we need first to model the effect of the laser on the floating particles.

### B. Modelling

To model the effect of the laser-generated flow, we propose a simplified dynamic model based on the flow study. As we have shown in a previous study [28], the interfacial flow direction is always away from the laser spot. On the other hand, the interfacial flow velocity is (approximately) inversely proportional to the distance from the laser spot. Based on these results, we propose the system model:

$$\tau\ddot{\mathbf{P}} + \dot{\mathbf{P}} = \alpha\frac{\mathbf{P} - \mathbf{L}}{\|\mathbf{P} - \mathbf{L}\|^2},\tag{1}$$

where $\mathbf{P} = (P_x, P_y)$ is the particle position, $\mathbf{L} = (L_x, L_y)$ is the laser spot position, and $\tau$ and $\alpha$ are fitting parameters. The parameter $\tau$ defines the system response time, due to all the system inertias (thermal, fluid, and particle), and $\alpha$ represents the strength of the thermocapillary actuation, which depends on the laser power and particle properties. Although an analytical expression for $\alpha$ cannot be established, we have shown [28] that the flow velocity scales with the squared root of the laser power.

The dynamic system (1) is non-linear and for any finite value of $\mathbf{P} - \mathbf{L}$, there are no equilibrium points (defined as those conditions to obtain $\ddot{\mathbf{P}} = \dot{\mathbf{P}} = 0$), which makes necessary the implementation of closed-loop control to stabilize the position. On the other hand, to obtain a constant velocity ($\ddot{\mathbf{P}} = 0$), it suffices to keep $\mathbf{P} - \mathbf{L}$ constant.

### C. Linearization

A first step toward the development of a controller for (1) is its linearization. The non-linear system (1) can be simplified by defining a new variable, the control velocity $\mathbf{C} = (C_x, C_y)$, as

$$\mathbf{C} = \alpha\frac{\mathbf{P} - \mathbf{L}}{\|\mathbf{P} - \mathbf{L}\|^2}.\tag{2}$$

Consequently, considering $\mathbf{C}$ as the input and $\mathbf{P}$ as the output, the system can be described by:

$$\tau\ddot{\mathbf{P}} + \dot{\mathbf{P}} = \mathbf{C},\tag{3}$$
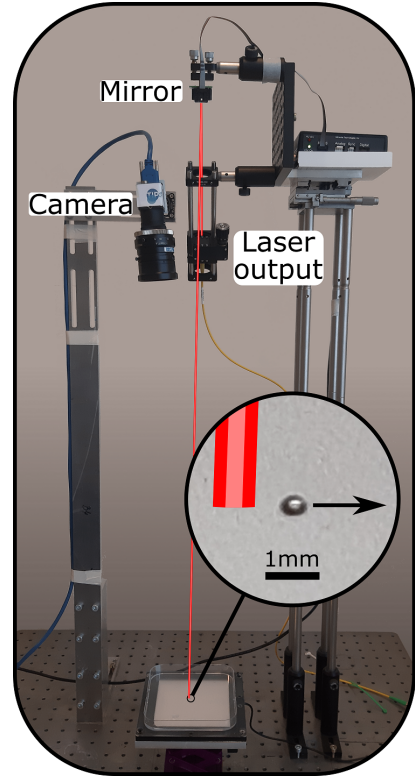


Fig. 1. Picture of the experimental setup in which an infra-red laser is used for flow generation. The red line drawn in the picture shows an example of the infrared laser beam. The inset is a picture of the floating metallic bead.
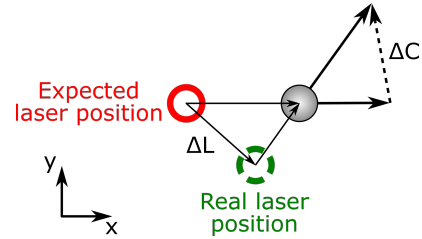


Fig. 2. Schematics showing the difference between the expected and real response ($\Delta\mathbf{C}$) of the system upon an error on the laser spot positioning ($\Delta\mathbf{L}$) due, for example, to a bad calibration of the mirror.

which is linear and can be controlled by traditional linear controllers. Then, the necessary laser spot position can be computed inverting (2) as

$$\mathbf{L} = \mathbf{P} - \alpha\frac{\mathbf{C}}{\|\mathbf{C}\|^2}.\tag{4}$$

Although this strategy allows us to circumvent the nonlinearity of the system, the results are highly sensitive to laser positioning errors. Indeed, if the real particle-laser relative position differs from the expected one, the resulting applied control input $\mathbf{C}$ will also differ from the expected one, as shown in Fig. 2. We call the difference in laser spot position $\Delta\mathbf{L}$, and the difference in input $\Delta\mathbf{C}$. Notice that for the same $\Delta\mathbf{L}$, $\Delta\mathbf{C}$ can become significantly large for small $\|\mathbf{P} - \mathbf{L}\|$. Therefore, a first measure to limit $\Delta\mathbf{C}$ is to keep the laser at a minimum distance $\|\mathbf{P} - \mathbf{L}\| > d_{\min}$, thus limiting the control velocity

to $\|\mathbf{C}\| < C_{\max} = \alpha/d_{\min}$. To compensate for the remaining uncertainty, we developed a non-linear laser position observer.

## III. CONTROL STRATEGY

For the closed-loop control of the non-linear system (1), we propose a new controller composed of a non-linear laser position observer and a linear position stabilization controller.

### A. Laser position observer

One way to eliminate laser position errors would be to measure and correct the real laser position. However, measuring the real position of the spot on the interface can be challenging since the infrared laser cannot be detected with a standard camera. Instead, we propose to use the measured particle response to estimate the real laser position. In particular, we propose to compensate for the laser positioning error by adding an estimation of this error to (4), obtaining:

$$\mathbf{L} = \mathbf{P} - \alpha \frac{\mathbf{C}}{\|\mathbf{C}\|^2} + \hat{\Delta \mathbf{L}}, \tag{5}$$

where $\hat{\Delta \mathbf{L}}$ is the estimated laser position error, based on the measured particle response.

For a constant velocity $\dot{\mathbf{P}}$, we could estimate the real laser spot position by inverting (1) as

$$\mathbf{L}_{\mathrm{est}} = \alpha \frac{\dot{\mathbf{P}}}{\|\dot{\mathbf{P}}\|^2}, \tag{6}$$

where $\dot{\mathbf{P}}$ is the measured particle velocity. This estimation has several limitations. First, its uncertainty becomes larger for lower measured velocities. Second, the parameter $\alpha$ in (1) can be difficult to estimate accurately, since it strongly depends on the experimental conditions (immersion height of the particle, surface contamination, etc.). Additionally, there could be other sources of noise and velocity fluctuations that would lead to erroneous estimations.

To attenuate the effect of all the mentioned uncertainties, we propose to add the correction gradually as

$$\hat{\Delta \mathbf{L}} = K_{obs} \int_0^t \mathbf{C}_{obs} \, dt, \tag{7}$$

where $K_{obs}$ is a gain, and we call $\mathbf{C}_{obs}$ the correction velocity. To account for the uncertainty of the laser position estimation, we compute $\mathbf{C}_{obs}$ differently in different cases:

1) If the measured velocity is small ($\|\dot{\mathbf{P}}\| < U_{\mathrm{thr}}$), the uncertainty in the estimation of $\mathbf{L}_{\mathrm{est}}$ is too large to be used in the observer. Therefore,
   a) if the control velocity is $\|\mathbf{C}\| < U_{\mathrm{thr}}$, we perform no further correction ($\mathbf{C}_{obs} = 0$).
   b) if the control velocity is $\|\mathbf{C}\| > U_{\mathrm{thr}}$, most probably the laser is further apart than expected. In this case, we take $\mathbf{C}_{obs} = \mathbf{C}$ to approach the laser spot to the particle.
2) If the measured velocity is $\|\dot{\mathbf{P}}\| > U_{\mathrm{thr}}$ and
   a) the difference between the expected and measured velocity magnitudes is low:

$$\left| \frac{\|\mathbf{C}\| - \|\dot{\mathbf{P}}\|}{\|\mathbf{C}\|} \right| < 0.5,$$

we assume the magnitude difference to be due to modeling errors. Therefore, the correction is only based on the orientation difference between the control and measured velocities:

$$\mathbf{C}_{obs} = \|\mathbf{C}\| \frac{\dot{\mathbf{P}}}{\|\dot{\mathbf{P}}\|} - \mathbf{C}.$$

In this case, notice that if $\dot{\mathbf{P}}$ and $\mathbf{C}$ are parallel, then $\mathbf{C}_{obs} = 0$.
   b) the difference between the expected and measured velocity magnitudes is high (above $50\%$), we compute $\mathbf{C}_{obs}$ as a function of the laser spot position error (using the estimation (6)) and velocity error as:

$$\mathbf{C}_{obs} = \|\dot{\mathbf{P}} - \mathbf{C}\| \frac{\mathbf{L}_{\mathrm{est}} - \mathbf{L}}{\|\mathbf{L}_{\mathrm{est}} - \mathbf{L}\|}.$$

The objective is to move the laser spot in the direction of the laser position error, with a velocity equal to the velocity error. As a result, the correction will be applied faster when the laser positioning error has a larger impact on the system response.

### B. Position stabilization

Pushing the particle in a desired direction using a repulsive effect results straight forward. Position stabilization, however, requires the implementation of closed-loop control since there are no equilibrium points. To achieve 2D stabilization, we decompose the problem into two independent controllers, one for each axis. To stabilize the particle position around a target $\mathbf{R} = (R_x, R_y)$, the control velocity is computed as a function of the error $\mathbf{E} = (E_x, E_y) = \mathbf{R} - \mathbf{P}$ as

$$\mathbf{C} = K_P \mathbf{E} + K_I \int_0^t \mathbf{E} \, dt. \tag{8}$$

With this controller, the error dynamics in the linear regime are:

$$\tau \ddot{\mathbf{E}} + \dot{\mathbf{E}} = -\left( K_P \mathbf{E} + K_I \int_0^t \mathbf{E} \, dt \right),$$

which converges to zero if $0 < \tau K_I < K_P$.

Then, we propose to couple the position stabilization controller (8) with the laser position observer (5) and (7) as shown Fig. 3.

## IV. EXPERIMENTAL VALIDATION

### A. Experimental implementation

To validate the controller, we focused on the control of $500\,\mu\mathrm{m}$ diameter steel spheres floating (thanks to surface tension [30]) on the surface of an initially still water layer. Then, we locally heat the interface from above using an infrared laser (wavelength $1455\,\mathrm{nm}$ and power $38\,\mathrm{mW}$), as shown in Fig. 1. The laser spot was displaced on the interface using a piezoelectric tip/tilt mirror. Finally, a camera was used to obtain the particles' position through visual feedback.

We empirically fitted the parameters $\tau$ and $\alpha$ in (1) for these particular conditions. First, we measured the particle velocity evolution upon suddenly approaching the laser spot
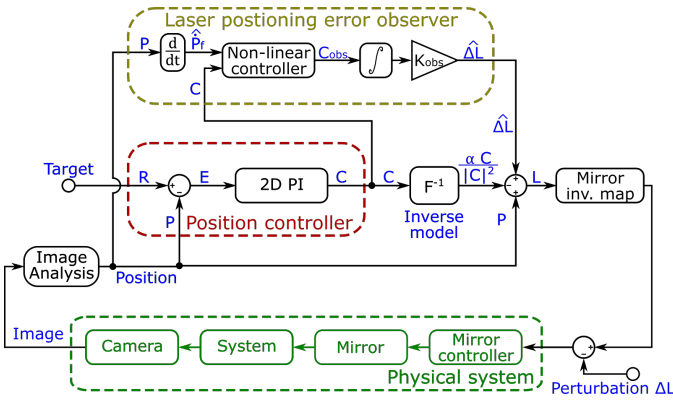
Fig. 3. Controller block diagram. The objective is to drive the particle position (**P**) to the reference position (**R**) using the laser spot position (**L**) as the control variable. The controller consists of two main blocks. The position controller defines the necessary actuation velocity (**C**) to drive the particle to the target. The laser position observer adjusts the laser position based on the discrepancy between the expected and measured response.
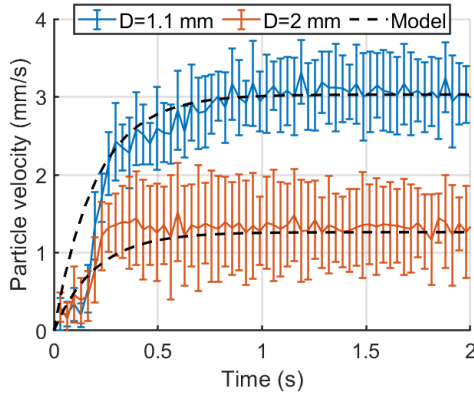


Fig. 4. Particle's velocity magnitude as a function of time for a laser-particle distance $d_L$ of $1.1\,\mathrm{mm}$ and $2\,\mathrm{mm}$, and a laser power $P_L = 38\,\mathrm{mW}$. Each point is the average of eight measurements. We fit (1) to $\tau = 0.2\,\mathrm{s}$.

to the particle and then keeping a constant relative position. We used the results, shown in Fig. 4, to fit $\tau \approx 0.2\,\mathrm{s}$. Then, we measured the particle steady-state velocity for different particle-laser distances. We used the results, shown in Fig. 5, to fit $\alpha \approx 2.5\,\mathrm{mm}^2/\mathrm{s}$. We can also estimate the resulting force acting on a still sphere as

$$\mathbf{F}_{\mathrm{th}} = m\ddot{\mathbf{P}} = m\frac{\alpha}{\tau}\frac{\mathbf{P}-\mathbf{L}}{\|\mathbf{P}-\mathbf{L}\|^2}.$$

For $\|\mathbf{P}-\mathbf{L}\| = 1\,\mathrm{mm}$, we estimate $\|\mathbf{F}_{\mathrm{th}}\| \approx 6\,\mathrm{nN}$.

Once our model's parameters were identified, we implemented the control algorithms in the experimental setup. The controller runs on a desktop computer which is connected to the camera and the mirror controller. The controller consists of an image analysis algorithm to obtain the particle position, the laser position observer, the position controller, and the mirror inverse map. The mirror inverse map computes the required mirror inputs to drive the laser to (approximately) the computed position. The complete schema of the controller is shown in Fig. 3. The experimental results are presented in the following sections.
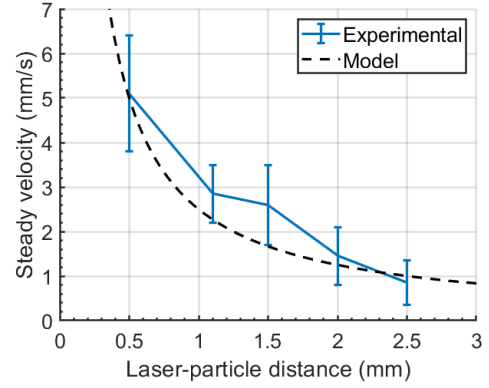


Fig. 5. Particle steady velocity magnitude as a function of the laser-particle distance for a laser power $P_L = 38\,\mathrm{mW}$. Each point is the average of eight measurements. We fit (1) to $\alpha = 2.5\,\mathrm{mm}^2/\mathrm{s}$.
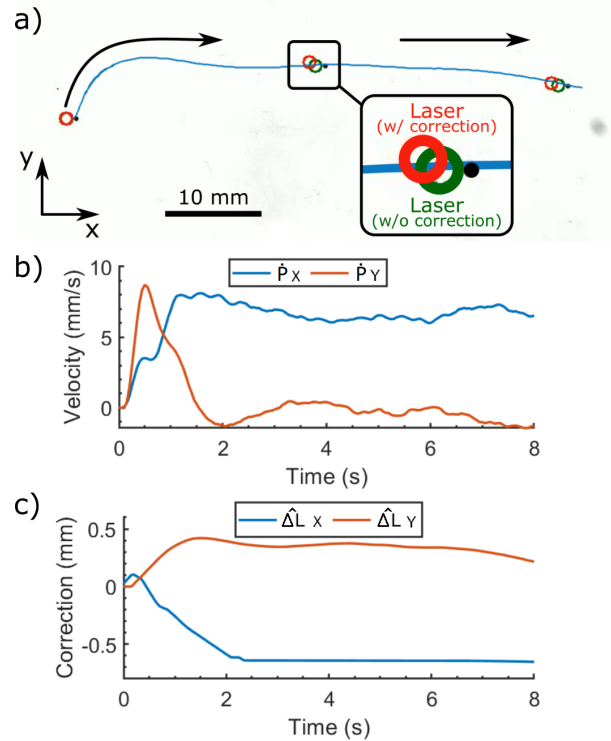


Fig. 6. Experimental sphere velocity control. (**a**) Trajectories under constant actuation velocity **C**. The red and green circle represents the requested laser position with and without the positioning correction, respectively. (**b**) Observed sphere velocity. (**c**) Evolution of the Laser position observer's (5) correction.

### B. Laser position observer result

To implement the laser position observer presented in Section III-A, we need to measure the particle velocity. To reduce the velocity estimation noise, we implemented an infinite impulse response filter to estimate the velocity based on position measurements. Then, we implemented the laser position observer with $K_{obs} = 0.1$ and $U_{\mathrm{thr}} = 1\,\mathrm{mm/s}$. The experimental results of the implemented observer under a constant control velocity (**C**) are shown in Fig. 6. It can be seen that the initial sphere velocity $\dot{\mathbf{P}}$ was misaligned with **C**, but the laser position observer corrects it in around $2\,\mathrm{s}$.
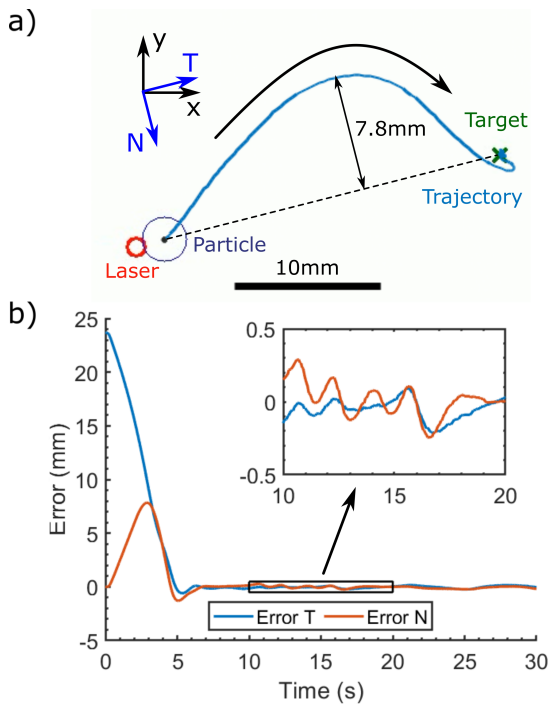
Fig. 7. Experimental sphere position stabilization without laser positioning error compensation. (**a**) The trajectory of the particle and its deviation from the straight line. See supplementary video. (**b**) Error evolution in the 'T' (toward the target) and 'N' (normal) axis. The error in 'N' increases up to $8\,\text{mm}$ due to the uncontrolled advancement direction.



Fig. 8. Experimental sphere position stabilization with laser positioning error compensation. (**a**) The trajectory of the particle moving between targets and its deviation from the straight line. See supplementary video. (**b**) Error evolution in the 'T' (toward the target) and 'N' (normal) axis. The error in 'N' remains close to zero (maximum $1.6\,\text{mm}$).

### C. Position stabilization result

The position stabilization controller (8) was implemented experimentally with gains $K_P = 0.5\,\text{s}^{-1}$ and $K_I = 0.5\,\text{s}^{-2}$.

First, we consider the results without the laser positioning error compensation ($K_{obs} = 0$), which are shown in Fig. 7. In that case, the sphere reaches the target and is stabilized around it. The integral action helped to stabilize the particle with a precision of $0.3\,\text{mm}$ (4 pixels). However, the trajectory deviates from the optimal straight line, with a maximum distance in the normal direction of $7.8\,\text{mm}$.

Then, we coupled the laser position observer with the position stabilization controller ($K_{obs} = 0.1$). The results are shown in Fig. 8, where it can be seen that the sphere advancement direction is initially erroneous, but the laser position observer quickly compensates for it. In the first movement, the error in the normal direction is limited to $1.6\,\text{mm}$ (5-fold decrease with respect to Fig. 7). Moreover, upon a change in the target, the correction previously found by the laser position observer remains valid and the sphere starts moving toward the new target in a straight trajectory. In the following movements, the deviation from the straight line is limited to $0.7\,\text{mm}$ (10-fold decrease with respect to Fig. 7).

## V. DISCUSSION

In this work, we propose an advanced control strategy for a particle actuated by a laser-powered thermocapillary micro-manipulation platform. To stabilize this inherently nonlinear system, closed-loop control algorithms are necessary. Although position stabiliza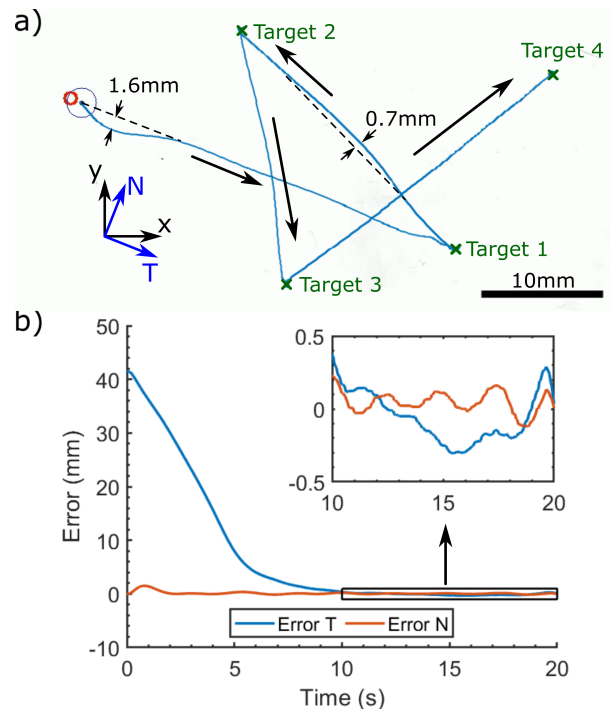tion can be achieved by linearizing the dynamic system and implementing a simple 2D proportional-integral controller, the nonlinearity of the system can amplify uncertainties and alter the system response. In particular, a linear controller would not be able to compensate for laser positioning errors, which can alter the particle's trajectory.

In a previous work [27], errors in the positioning of the laser and the incapability to compensate for them hindered the transient performance of position controllers. In this work, we propose using a nonlinear observer to estimate and compensate for any laser position error. This observer estimates the real laser spot position from the particle response and compensates for deviations. We have experimentally implemented a position controller and investigated the system response with and without the laser position error compensation. Without compensation, the particle reaches the target but takes an inefficient convoluted path. With compensation, on the other hand, the particle moves in an almost straight line between targets, reducing the total traveled distance.

One disadvantage of our proposed strategy (nonlinear laser position observer and linear position controller) is that their dynamics could interfere. However, this is generally not the case since the error is normally large enough at the beginning to saturate the position controller, thus keeping **C** mostly constant for the first few seconds and giving time for the laser position observer to settle. On the other hand, the main advantage of this approach is that it considers the nonlinearity of the system, making it more robust to larger laser positioning errors than a simple position controller.

In conclusion, our developed strategy represents an advance

over previous algorithms since, after an initial settling time, it improves the transient response (10-fold decrease in the deviation from a linear trajectory). Additionally, the spatial selectivity of the actuation system enables the extension of the algorithm for the simultaneous control of multiple particles using multiple laser spots. If the particles are sufficiently far apart, they can be actuated independently of each other [27]. If they are closer, the flows can interfere and affect the other particles. A future extension of this work would be the development of a controller that considers the presence of other particles to find the best position for the laser spots.

## Acknowledgment

## References

[1] M. Gauthier, S. Régnier, P. Rougeot, and N. Chaillet, "Analysis of forces for micromanipulations in dry and liquid media." *Journal of Micromechatronics*, vol. 3, no. 3-4, pp. 389–413, 2006.

[2] J. Li, I. Rozen, and J. Wang, "Rocket science at the nanoscale," *ACS Nano*, vol. 10, no. 6, pp. 5619–5634, 2016.

[3] A. Pena-Francesch, J. Giltinan, and M. Sitti, "Multifunctional and biodegradable self-propelled protein motors," *Nature Communications*, vol. 10, no. 1, pp. 1–10, 2019.

[4] V. Sridhar, B.-W. Park, S. Guo, P. A. van Aken, and M. Sitti, "Multiwavelength-steerable visible-light-driven magnetic coo–tio2 microswimmers," *ACS Applied Materials & Interfaces*, vol. 12, no. 21, pp. 24 149–24 155, 2020.

[5] M. Kaynak, P. Dirix, and M. S. Sakar, "Addressable acoustic actuation of 3d printed soft robotic microsystems," *Advanced Science*, vol. 7, no. 20, p. 2001120, 2020.

[6] S. Mohanty, A. Paul, P. M. Matos, J. Zhang, J. Sikorski, and S. Misra, "Ceflowbot: A biomimetic flow-driven microrobot that navigates under magneto-acoustic fields," *Small*, vol. 18, no. 9, p. 2105829, 2022.

[7] A. Aghakhani, A. Pena-Francesch, U. Bozuyuk, H. Cetin, P. Wrede, and M. Sitti, "High shear rate propulsion of acoustic microrobots in complex biological fluids," *Science Advances*, vol. 8, no. 10, p. eabm5126, 2022.

[8] A. Oulmas, N. Andreff, and S. Régnier, "3d closed-loop swimming at low reynolds numbers," *The International Journal of Robotics Research*, vol. 37, no. 11, pp. 1359–1375, 2018.

[9] Z. Wu, J. Troll, H.-H. Jeong, Q. Wei, M. Stang, F. Ziemssen, Z. Wang, M. Dong, S. Schnichels, T. Qiu, *et al.*, "A swarm of slippery micropropellers penetrates the vitreous body of the eye," *Science Advances*, vol. 4, no. 11, p. eaat4388, 2018.

[10] X.-Z. Chen, J.-H. Liu, M. Dong, L. Müller, G. Chatzipirpiridis, C. Hu, A. Terzopoulou, H. Torlakcik, X. Wang, F. Mushtaq, *et al.*, "Magnetically driven piezoelectric soft microswimmers for neuron-like cell delivery and neuronal differentiation," *Materials Horizons*, vol. 6, no. 7, pp. 1512–1516, 2019.

[11] X. Li and C. C. Cheah, "Robotic cell manipulation using optical tweezers with unknown trapping stiffness and limited fov," *IEEE/ASME Transactions on Mechatronics*, vol. 20, no. 4, pp. 1624–1632, 2014.

[12] M. Xie, Y. Wang, G. Feng, and D. Sun, "Automated pairing manipulation of biological cells with a robot-tweezers manipulation system," *IEEE/ASME Transactions on Mechatronics*, vol. 20, no. 5, pp. 2242–2251, 2014.

[13] E. Gerena, S. Régnier, and S. Haliyo, "High-bandwidth 3-d multitrap actuation technique for 6-dof real-time control of optical robots," *IEEE Robotics and Automation Letters*, vol. 4, no. 2, pp. 647–654, 2019.

[14] M. Baudoin and J.-L. Thomas, "Acoustic tweezers for particle and fluid micromanipulation," *Annual Review of Fluid Mechanics*, vol. 52, no. 1, 2019.

[15] Z. Ma, K. Melde, A. G. Athanassiadis, M. Schau, H. Richter, T. Qiu, and P. Fischer, "Spatial ultrasound modulation by digitally controlling microbubble arrays," *Nature Communications*, vol. 11, no. 1, pp. 1–7, 2020.

[16] A. Kopitca, K. Latifi, and Q. Zhou, "Programmable assembly of particles on a chladni plate," *Science Advances*, vol. 7, no. 39, p. eabi7716, 2021.

[17] M. Dkhil, M. Kharboutly, A. Bolopion, S. Régnier, and M. Gauthier, "Closed-loop control of a magnetic particle at the air–liquid interface," *IEEE Transactions on Automation Science and Engineering*, vol. 14, no. 3, pp. 1387–1399, 2015.

[18] F. Ongaro, S. Pane, S. Scheggi, and S. Misra, "Design of an electromagnetic setup for independent three-dimensional control of pairs of identical and nonidentical microrobots," *IEEE Transactions on Robotics*, vol. 35, no. 1, pp. 174–183, 2018.

[19] J. Giltinan and M. Sitti, "Simultaneous six-degree-of-freedom control of a single-body magnetic microrobot," *IEEE Robotics and Automation Letters*, vol. 4, no. 2, pp. 508–514, 2019.

[20] A. Barbot, H. Tan, M. Power, F. Seichepine, and G.-Z. Yang, "Floating magnetic microrobots for fiber functionalization," *Science Robotics*, vol. 4, no. 34, p. eaax8336, 2019.

[21] M. Tanyeri and C. M. Schroeder, "Manipulation and confinement of single particles using fluid flow," *Nano Letters*, vol. 13, no. 6, pp. 2357–2364, 2013.

[22] A. Shenoy, C. V. Rao, and C. M. Schroeder, "Stokes trap for multiplexed particle manipulation and assembly using fluidics," *Proceedings of the National Academy of Sciences*, vol. 113, no. 15, pp. 3976–3981, 2016.

[23] M. D. Armani, S. V. Chaudhary, R. Probst, and B. Shapiro, "Using feedback control of microflows to independently steer multiple particles," *Journal of Microelectromechanical systems*, vol. 15, no. 4, pp. 945–956, 2006.

[24] T. Hayakawa, S. Sakuma, and F. Arai, "Cell manipulation method based on vibration-induced local flow control in open chip environment," in *2015 28th IEEE International Conference on Micro Electro Mechanical Systems (MEMS)*. IEEE, 2015, pp. 200–203.

[25] F. N. P. Basualdo, G. Gardi, W. Wang, S. O. Demir, A. Bolopion, M. Gauthier, P. Lambert, and M. Sitti, "Control and transport of passive particles using self-organized spinning micro-disks," *IEEE Robotics and Automation Letters*, vol. 7, no. 2, pp. 2156–2161, 2022.

[26] R. Terrazas, A. Bolopion, J.-C. Beugnot, P. Lambert, and M. Gauthier, "Closed-loop particle motion control using laser-induced thermocapillary convective flows at the fluid/gas interface at micrometric scale," *IEEE/ASME Transactions on Mechatronics*, vol. 23, no. 4, pp. 1543–1554, 2018.

[27] F. N. P. Basualdo, A. Bolopion, M. Gauthier, and P. Lambert, "A microbotic platform actuated by thermocapillary flows for manipulation at the air-water interface," *Science Robotics*, vol. 6, no. 52, 2021.

[28] F. N. Piñan Basualdo, R. Terrazas Mallea, B. Scheid, A. Bolopion, M. Gauthier, and P. Lambert, "Effect of insoluble surfactants on a thermocapillary flow," *Physics of Fluids*, vol. 33, no. 7, 2021.

[29] L. Scriven and C. Sternling, "The Marangoni effects," *Nature*, vol. 187, no. 4733, pp. 186–188, 1960.

[30] D. Vella, "Floating versus sinking," *Annual Review of Fluid Mechanics*, vol. 47, pp. 115–135, 2015.